EMHD flow of non-Newtonian nanofluids over thin needle with Robinson's condition and Arrhenius pre-exponential factor law

To cite this article: Fazle Mabood *et al* 2020 *Phys. Scr.* **95** 115219

View the article online for updates and enhancements.

EMHD flow of non-Newtonian nanofluids over thin needle with Robinson's condition and Arrhenius pre-exponential factor law

Fazle Mabood[1] , **Taseer Muhammad**[2], **M K Nayak**[3], **Hassan Waqas**[4] and **O D Makinde**[5]

[1] Department of Information Technology, Fanshawe College London ON, Canada
[2] Department of Mathematics, College of Sciences, King Khalid University, Abha 61413, Saudi Arabia
[3] Department of Physics, IHSE, Siksha 'O' Anusandhan Deemed to be University, Bhubaneswar-751003, India
[4] Department of Mathematics, Government College University Faisalabad, Layyah Campus 31200, Pakistan
[5] Faculty of Military Science, Stellenbosch University, Private Bag X2, Saldanha 7395, South Africa

E-mail: tasgher@kku.edu.sa and taseer_qau@yahoo.com

CrossMark

Abstract

Many researchers and scientists are devoting their time to scrutinize nanofluids nature and characteristics for heat transfer enhancement. The scrutiny of nanoliquids is important in the large scale thermal management systems via evaporators, advanced cooling systems, heat exchangers, micro/nano-electromechanical devices and industrial chilling applications. Nanoliquids are very momentous even in the natural process via different fields like chemistry, chemical engineering, physics and biology. Nanoliquids can be utilized in various fields of engineering such as different chemical procedures, cooling of electronic equipment and heat exchangers. The main aim of current article is to scrutinize electromagnetohydrodynamic flow of micropolar-Casson-Carreau nanoliquids over thin needle with Robinson's conditions and Arrhenius pre-exponential factor law. Double stratification effects are also taken into account. The reverent partial differential equations are reformulated into the system of ordinary differential expressions by implementing appropriate transformations. Such obtained equations subject to boundary constraints are computed numerically by considering Runge–Kutta-Fehlberg method. Behaviour of numerous interesting parameters on flow fields is deliberated. The outcomes of flow fields are delineated through graphs and tabular data.

Keywords: electromagnetohydrodynamic flow, double stratification, non-Newtonian nanofluids, Robinson's conditions, Arrhenius pre-exponential factor law, Thin needle

(Some figures may appear in colour only in the online journal)

1. Introduction

Nanofluids include nanomaterials of less than 100 nm of suspension diameter that are utilized for improvement of thermal conductivity. Applications of the nanofluids are used for electric heating water, increased storage, refrigerator, condenser heat transfer performance and efficient solar power absorption. The novel characteristics of nanoliquids include impressive heat transport and thermal conductivity enhancements. Recent survey depicts a significant increase in the applications of nanoliquids in the several kinds of micro-systems such as microchannels, micro heat pipes and micro-reactors. There is further significant potential in utilizing the nanoliquids in the medical sciences like bio-separation systems, enzyme biosensors, biomimetic microsystems and drug delivery systems. Nanofluids are used in the cooling of industrial machines, nuclear plants, transformer oils and nanoelectronic.

Choi and Eastman [1] initiated nanofluid flow. Buongiorno [2] established the model of nanofluid flow together with
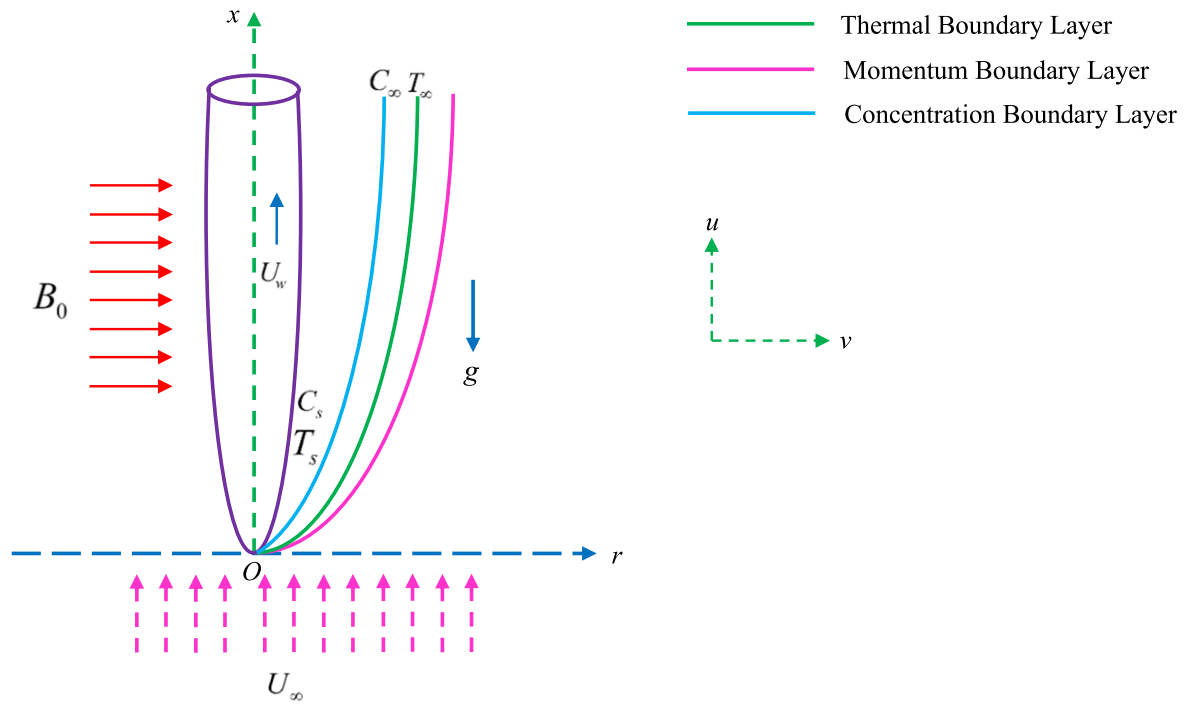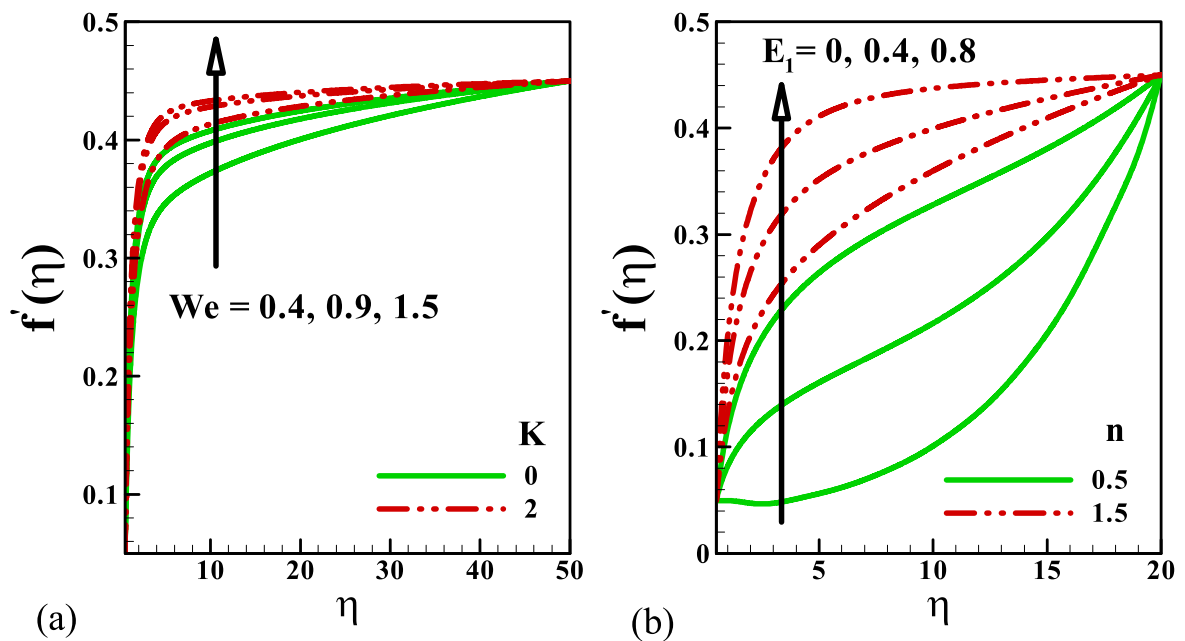
Figure 1. Flow representation of the problem.

Figure 2. Outcomes of *f′* versus (a) *We*, *K* (b) E_1, *n*.

Brownian motion and thermophoretic aspects. Ali *et al* [3] studied the development structure of cylinder for cross-liquid movement of nanoparticles in an electromagnetic environment. Shah *et al* [4] scrutinized Maxwell nanofluid movement between vertical sheets with heat flux and convection effects. Ahmed *et al* [5] examined the mixed convection effect in Maxwell nanoliquids 3D flow by vertical stretching cylinder. Hayat *et al* [6] addressed the stagnation point movement of

non-Newtonian liquid (Carreau liquid) by numerical simulation with Cattaneo-Christov thermal gradient. Tlili *et al* [7] discussed the 3D magnetohydrodynamic (MHD) Maxwell nanofluid flow with heat diffusion/generative impacts. Khan *et al* [8] explored boundary-layer movement of Maxwell nanoliquids through an extendable revolving cylinder subject to transverse magnetosphere. Riaz *et al* [9] investigated the MHD Maxwell liquid flow processing concerning local and non-local
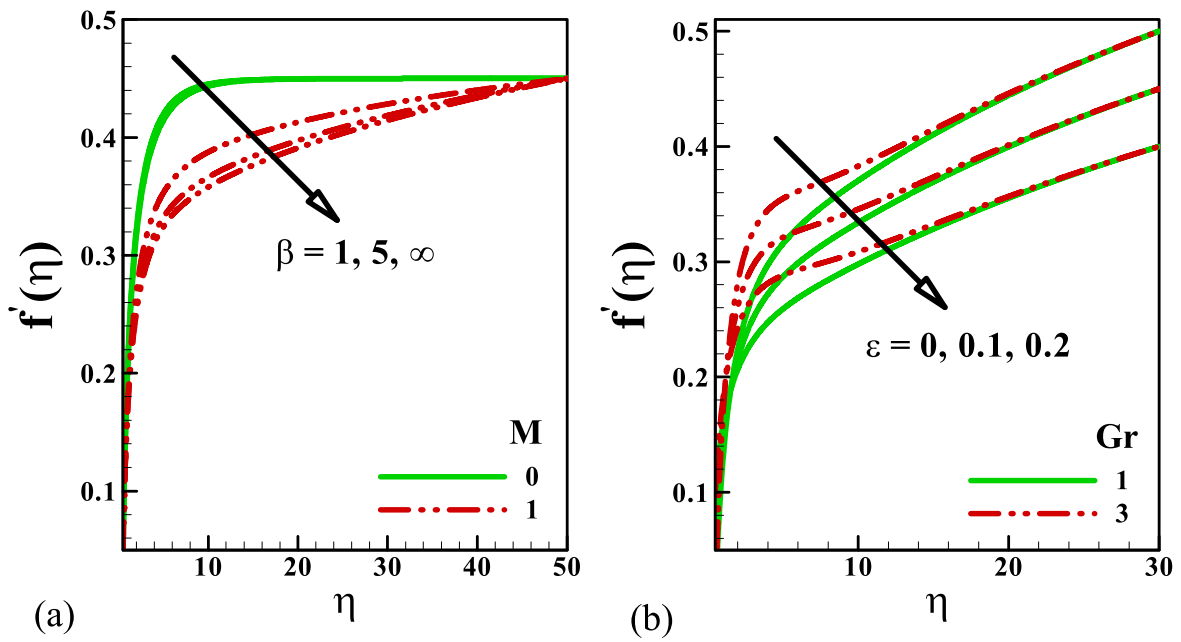
Figure 3. Outcomes of f' versus (a) β, M (b) Gr, ε.
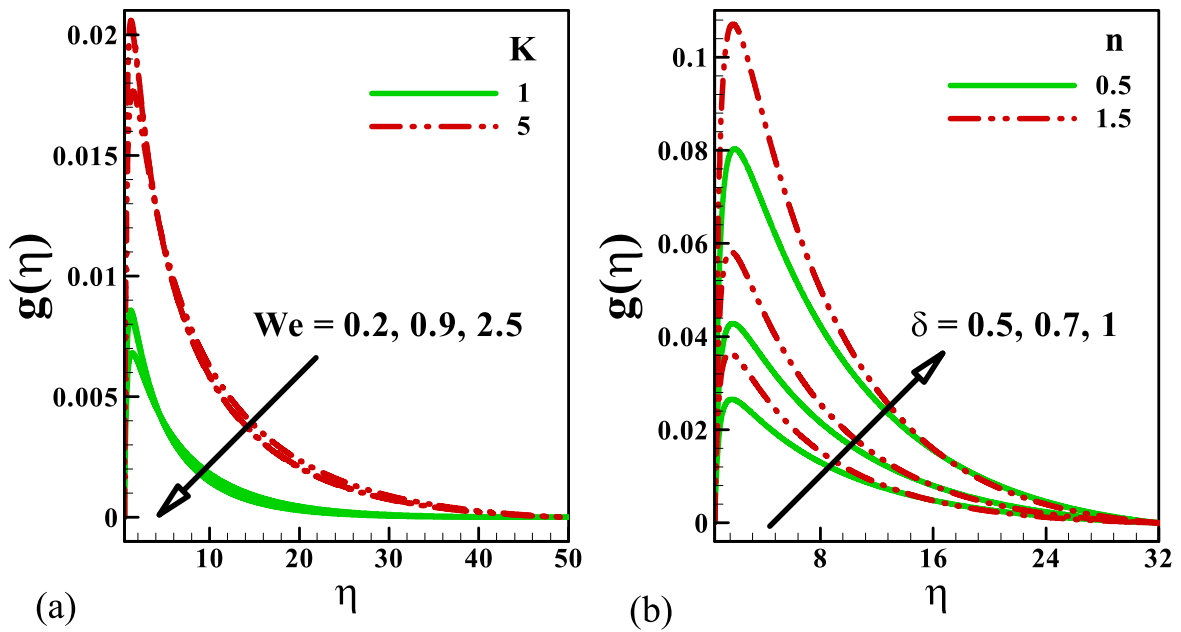

Figure 4. Outcomes of $g(\eta)$ versus (a) We, K (b) δ, n.

differentiated operators. Vahid *et al* [10] scrutinized boundary-layer nanoliquid flow and heat and mass transport over the surface. Hayat *et al* [11] addressed Carreau liquid peristaltic MHD flow in a medium of different waveforms. Ellahi *et al* [12] discussed the function of slipping in a two-phase movement of the Newtonian liquids. Shafee *et al* [13] investigated the simulation model for turbulent flow in a pipe via a hybrid swirling movement system that assumes nanofluid energy deficiency. Iftikhar *et al* [14] investigated the effect of ferromagnetic dipole on the flow of a nanofluid through a stretching cylinder. Raza [15] examined the cumulative impact of thermal radiation and velocity slip along with the convective heated

stretching sheet. Many researcher works on the nanofluids which are carried out via studies [16–33].

2. Mathematical formulation

Steady, incompressible electromagnetic micropolar-Casson-Carreau nanofluids flow over thin needle is discussed. Flow model and related coordinate systems are analyzed. A schematic diagram associated with the concerned problem is shown in figure 1.

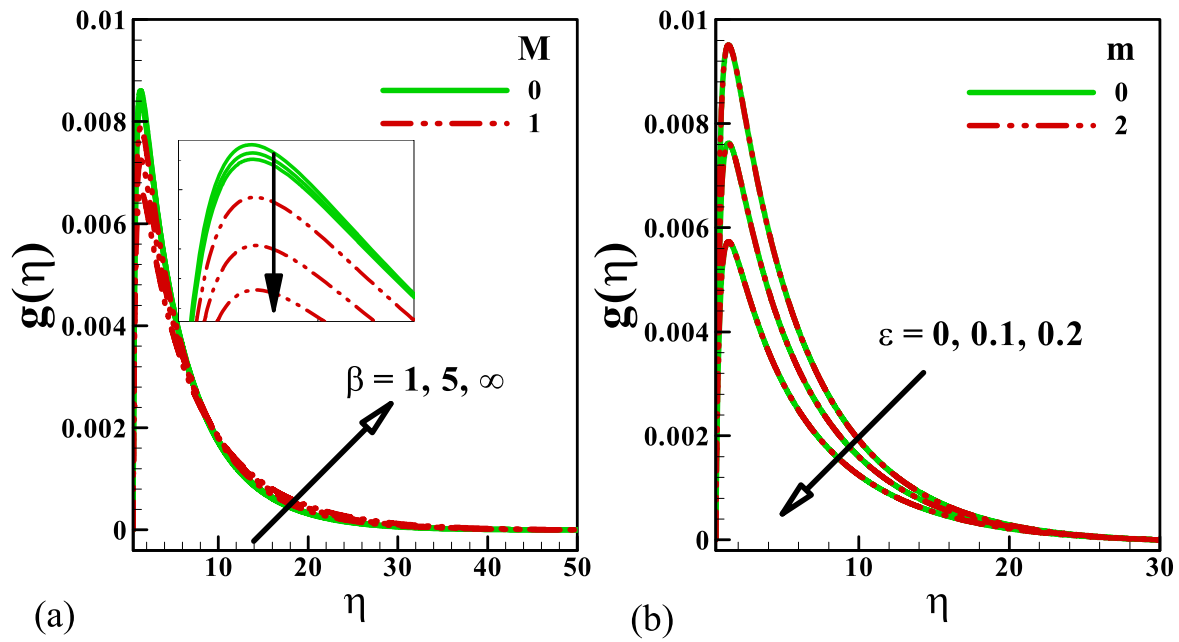In current paper, we have following restrictions:

Figure 5. Outcomes of $g(\eta)$ versus (a) β, M (b) m, ε.

(i) Thickness of needle is comparable/smaller than that of thermal and momentum boundary-layers over it.

(ii) Influence of curvature in transverse-direction has been prominent.

(iii) Pressure-gradient along thin needle is ignored i.e. $\frac{\partial p}{\partial x} = 0$.

(iv) Ohmic heating and viscous dissipation impacts are considered.

(v) Arrhenius pre-exponential factor law is introduced.

(vi) Robinson's conditions are implemented.

(vii) Catteneo Christov double diffusion theory is applied.

(viii) Micropolar fluid model is applied.

(ix) Casson and Carreau fluid models are implemented.

(x) Buongiorno model is implemented.

(xi) Electromagneto hydrodynamic flow model is included.

Under the above assumptions, the resulting equations of non-Newtonian nanofluids flow over thin needle are

$$\frac{\partial}{\partial x}(ru) + \frac{\partial}{\partial r}(rv) = 0, \qquad (1)$$

$$u\frac{\partial u}{\partial x} + v\frac{\partial u}{\partial r} = \left(\frac{\mu_f + k}{\rho_f}\right)\left(1 + \frac{1}{\beta}\right)$$

$$\times \left\{ \begin{array}{l} \left(\frac{1}{r}\frac{\partial u}{\partial r} + \frac{\partial^2 u}{\partial r^2}\right)\left[1 + \Gamma^2\left(\frac{\partial u}{\partial r}\right)^2\right]^{\frac{n-1}{2}} \\ + (n-1)\Gamma^2\left(\frac{\partial u}{\partial r}\right)^2\left(\frac{\partial^2 u}{\partial r^2}\right)\left[1 + \Gamma^2\left(\frac{\partial u}{\partial r}\right)^2\right]^{\frac{n-3}{2}} \end{array} \right\}$$

$$+ g^*\beta_T (T - T_\infty) + \frac{k}{\rho_f}\frac{\partial N}{\partial r} + \frac{\sigma_f}{\rho_f}(E_0 B_0 - B_0^2 u) \qquad (2)$$

$$\rho_f j\left(u\frac{\partial N}{\partial x} + v\frac{\partial N}{\partial r}\right) = \gamma\frac{\partial^2 N}{\partial r^2} - k\left(2N + \frac{\partial u}{\partial r}\right) \qquad (3)$$

$$u\frac{\partial T}{\partial x} + v\frac{\partial T}{\partial r} + \Omega_1$$

$$\times \left(\begin{array}{l} u^2\frac{\partial^2 T}{\partial x^2} + v^2\frac{\partial^2 T}{\partial r^2} + 2uv\frac{\partial^2 T}{\partial r\partial x} + u\frac{\partial u}{\partial x}\frac{\partial T}{\partial x} \\ + u\frac{\partial v}{\partial x}\frac{\partial T}{\partial r} + v\frac{\partial u}{\partial r}\frac{\partial T}{\partial x} + v\frac{\partial v}{\partial r}\frac{\partial T}{\partial r} \end{array} \right)$$

$$= \frac{\alpha_f}{r}\frac{\partial}{\partial r}\left(r\frac{\partial T}{\partial r}\right) + \frac{(\rho c_p)_p}{(\rho c_p)_f}\left[D_B\frac{\partial C}{\partial r}\frac{\partial T}{\partial r} + \frac{D_T}{T_\infty}\left(\frac{\partial T}{\partial r}\right)^2\right]$$

$$+ \left(1 + \frac{1}{\beta}\right)\frac{(\mu_f + k)}{(\rho c_p)_f}\left[1 + \Gamma^2\left(\frac{\partial u}{\partial r}\right)^2\right]^{\frac{n-1}{2}}\left(\frac{\partial u}{\partial r}\right)^2$$

$$+ \frac{\sigma_f}{(\rho c_p)_f}(u^2 B_0^2 - E_0^2) \qquad (4)$$

$$u\frac{\partial C}{\partial x} + v\frac{\partial C}{\partial r} + \Omega_2$$

$$\times \left(\begin{array}{l} u^2\frac{\partial^2 C}{\partial x^2} + v^2\frac{\partial^2 C}{\partial r^2} + 2uv\frac{\partial^2 C}{\partial r\partial x} + u\frac{\partial u}{\partial x}\frac{\partial C}{\partial x} \\ + u\frac{\partial v}{\partial x}\frac{\partial C}{\partial r} + v\frac{\partial u}{\partial r}\frac{\partial C}{\partial x} + v\frac{\partial v}{\partial r}\frac{\partial C}{\partial r} \end{array} \right)$$

$$= \frac{D_B}{r}\frac{\partial}{\partial r}\left(r\frac{\partial C}{\partial r}\right) + \frac{D_T}{T_\infty}\frac{1}{r}\frac{\partial}{\partial r}\left(r\frac{\partial T}{\partial r}\right) - K^* \qquad (5)$$

Here, u and v are the axial and radial components of velocity, (x, r) cylindrical coordinates, ρ_f density of fluid, μ_f fluid dynamic viscosity, k vortex viscosity of micro-polar fluid, β Casson fluid parameter, n power law index, Γ time constant, σ_f Stefan Boltzmann constant, k^* mean absorption coefficient, Ω_1 and Ω_2 thermal and solutal relaxation times correspondingly, (T, C) temperature and concentration of nanoparticles respectively and (T_∞, C_∞)
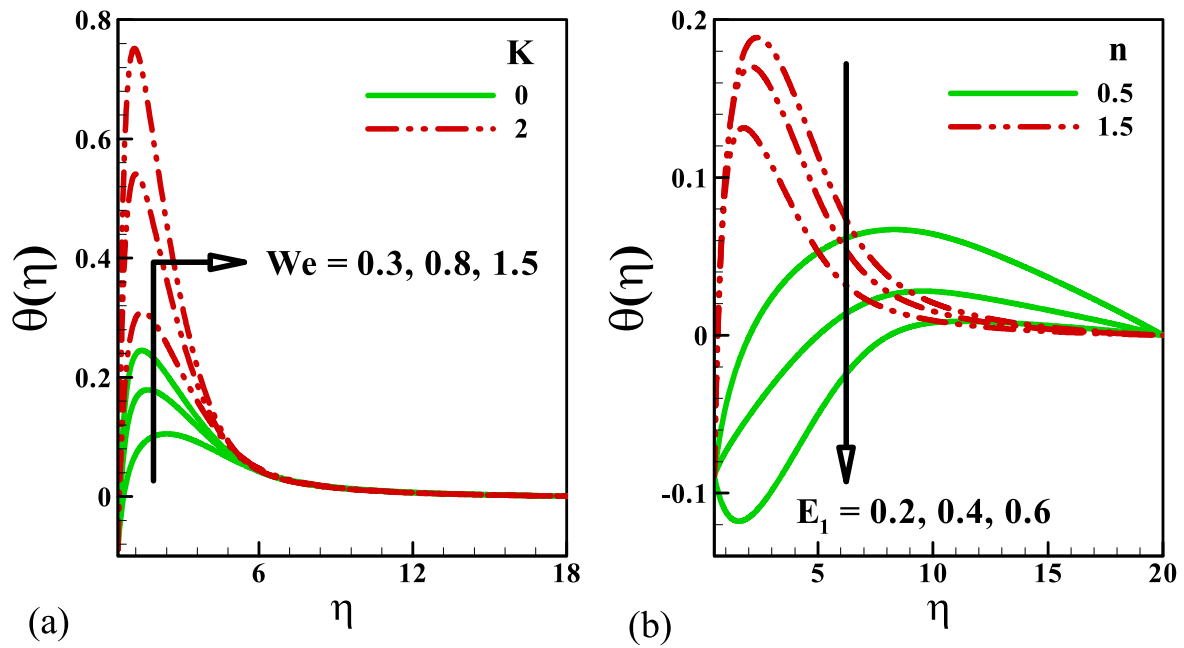
Figure 6. Outcomes of $\theta(\eta)$ versus (a) *We*, *K* (b) E_1, *n*.

ambient temperature and concentration of nanoparticles respectively. We assume that the spin gradient viscosity (γ) is addressed by

$$\gamma = \left(\mu_f + \frac{k}{2}\right)j = \mu_f\left(1 + \frac{K}{2}\right)j \qquad (6)$$

In which $K = \frac{k}{\mu_f}$ shows material parameter, α_f thermal diffusivity, g gravitational acceleration, β_T thermal expansion coefficient, D_B coefficient of mass diffusion, E_0 electric field strength and B_0 magnetic field strength.

In concentration expression (5), the expression $K* = k_r^2\left(\frac{T}{T_\infty}\right)^m \exp\left(-\frac{E_a}{k_BT}\right)$ expresses the Arrhenius Pre-exponential factor law. Here k_r^2 stands for chemical reaction rate constant, E_a for activation energy and $k_B = 1.38 \times 10^{-23}$J K^{-1} for Boltzman constant. Employing above information, equation (5) becomes

$$u\frac{\partial C}{\partial x} + v\frac{\partial C}{\partial r} + \Omega_2$$
$$\times \left(\begin{array}{c} u^2\frac{\partial^2 C}{\partial x^2} + v^2\frac{\partial^2 C}{\partial r^2} + 2uv\frac{\partial^2 C}{\partial r\partial x} + u\frac{\partial u}{\partial x}\frac{\partial C}{\partial x} \\ +u\frac{\partial v}{\partial x}\frac{\partial C}{\partial r} + v\frac{\partial u}{\partial r}\frac{\partial C}{\partial x} + v\frac{\partial v}{\partial r}\frac{\partial C}{\partial r} \end{array}\right)$$
$$= \frac{D_B}{r}\frac{\partial}{\partial r}\left(r\frac{\partial C}{\partial r}\right) + \frac{D_T}{T_\infty}\frac{1}{r}\frac{\partial}{\partial r}\left(r\frac{\partial T}{\partial r}\right)$$
$$\underbrace{- k_r^2\left(\frac{T}{T_\infty}\right)^m \exp\left(-\frac{E_a}{k_BT}\right)(C - C_\infty)}_{Arrhenius\ pre-\exp onential\ factor\ law} \qquad (7)$$

Boundary conditions for current problem are

$$\left.\begin{array}{l} u|_{r=R} = u_w, \; v|_{r=R} = 0, \; N|_{r=R} = -m\frac{\partial u}{\partial r}\Big|_{r=R} \\ -k\frac{\partial T}{\partial r} = h_1(T_s - T)|_{r=R}, \; -k\frac{\partial C}{\partial r} = h_2(C_s - C)|_{r=R} \\ u|_{r\to\infty} = u_\infty, \; N|_{r\to\infty} \to 0, \; T|_{r\to\infty} \to T_\infty = c_1x \\ \quad + T_0, \; C|_{r\to\infty} \to C_\infty = d_1x + C_0, \end{array}\right\} \quad (8)$$

here h_1 and h_2 stand for heat and mass transfer coefficients, $T_s = cx + T_0$, $C_s = dx + C_0$ for surface temperature-concentration and $T_\infty = c_1x + T_0$, $C_\infty = d_1x + C_0$ for ambient temperature-concentration respectively.

The suitable transformations are

$$\left.\begin{array}{l} u = 2Uf'(\eta), \; v = -\frac{v_f}{r}f + \eta\frac{v_f}{r}f'(\eta), \; N = \frac{rU^2}{v_fx}g(\eta), \\ \theta(\eta) = \frac{T - T_\infty}{T_s - T_0}, \; \phi(\eta) = \frac{C - C_\infty}{C_s - C_0}, \; \eta = \frac{Ur^2}{v_fx} \end{array}\right\} \quad (9)$$

where velocities u and v satisfy equation (1) identically. By letting $\eta = A$ in the equation (6), we have $R(x) = \left(\frac{Avx}{U}\right)^{1/2}$ is the surface shape of axisymmetric body. Using equation (9) in equations (2)–(5) and (8), we get

$$(1 + K)\left(1 + \frac{1}{\beta}\right)\left\{\begin{array}{l} (2f'' + 2\eta f''')(1 + 16\,We^2)^{\frac{n-1}{2}} \\ + 16(n-1)We^2(f'' + 2\eta f''')(1 + 16\,We^2)^{\frac{n-3}{2}} \end{array}\right\}$$
$$+ ff'' + \frac{1}{4}\left(\frac{Gr}{Re_x^2}\right)\theta + \frac{1}{4}K(g + 2\eta g') + \frac{1}{4}M(E_1 - 2f') = 0 \qquad (10)$$

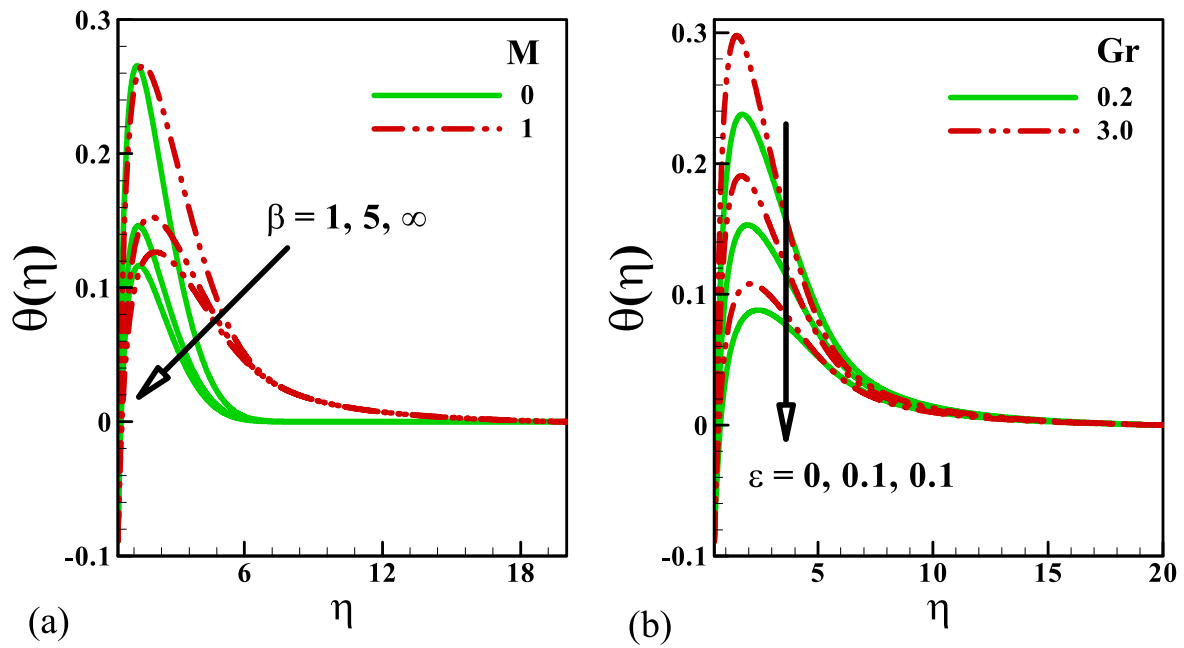**Figure 7.** Outcomes of $\theta(\eta)$ versus (a) β, M (b) G_r, ε.

$$\left(1 + \frac{K}{2}\right)(4\eta^2 g'' + 6\eta g') + \eta(2fg' + gf')$$
$$+ fg - 2KB(g + 2f'') = 0 \tag{11}$$

$$2\theta' + 2\eta\theta'' + \mathrm{Pr}f\theta'$$
$$- \mathrm{Pr}\Gamma_1 \left\{ \begin{array}{l} 4\eta^2 (f')^2\theta'' + 4\eta(f')^2\theta'' - 4\eta f\, f'\theta'' \\ +2\eta\Lambda f\, f'\theta'' - 3\eta f^2\theta' + \frac{2}{\eta}f^2\theta' \end{array} \right\}$$
$$+ 2\mathrm{Pr}\, Nb\, \eta\theta'\phi' + 2\mathrm{Pr}Nt\, \eta\, (\theta')^2$$
$$+ 8\left(1 + \frac{1}{\beta}\right)(1 + K)\eta Br(1 + 16\, We^2)^{\frac{n-1}{2}}(f'')^2$$
$$+ Br\, M\left\{ 2(f')^2 - \frac{1}{2}E_1^2 \right\} = 0 \tag{12}$$

$$2\phi' + 2\eta\phi'' + Sc\, f\phi'$$
$$- Sc\, \Gamma_2 \left\{ \begin{array}{l} 4\eta^2 (f')^2\phi'' + 4\eta(f')^2\phi'' - 4\eta f\, f'\phi'' \\ +2\eta\Lambda f\, f'\phi'' - 3\eta f^2\phi' + \frac{2}{\eta}f^2\phi' \end{array} \right\}$$
$$+ 2\left(\frac{Nt}{Nb}\right)(\theta' + \eta\theta'') - \frac{1}{2}\lambda\, Sc(1 + \delta\theta)^m \exp\left[-\frac{E}{(1 + \delta\theta)}\right]\phi = 0 \tag{13}$$

with

$$\left. \begin{array}{l} f'(A) = \dfrac{\varepsilon}{2}, f(A) = 0,\ g(A) = -4mf''(A), \\[2mm] \theta'(A) = -\dfrac{1}{2}\beta_1[1 - S_t - \theta(A)],\ \phi'(A) = -\dfrac{1}{2}\beta_2[1 - S_c - \phi(A)], \\[2mm] f'(\infty) = \dfrac{1}{2}(1 - \varepsilon),\ g'(\infty) = 0,\ \ \theta(\infty) \to 0,\ \ \phi(\infty) \to 0 \end{array} \right\} \tag{14}$$

In the above expressions, the involved interesting parameters are defined by

$$\left. \begin{array}{l} \mathrm{Re}_x = \dfrac{Ux}{\upsilon_f},\ We = \left(\dfrac{\Gamma U}{x}\right)\mathrm{Re}_x,\ K = \dfrac{k}{\mu_f},\ E_1 = \dfrac{U_0}{EB_0},\ M = \dfrac{\sigma_f B_0^2 x}{\rho_f U},\ Sc = \dfrac{\upsilon_f}{D_B},\ B = \dfrac{r^2}{j}, \\[3mm] \delta = \dfrac{T_s - T_0}{T_\infty},\ Gr = \dfrac{g^*\beta(T_s - T_0)x^3}{\upsilon_f^2},\ \Gamma_1 = \dfrac{\Omega_1 U}{x},\ \Gamma_2 = \dfrac{\Omega_2 U}{x},\ \mathrm{Pr} = \dfrac{\upsilon_f}{\alpha_f},\ \Lambda = \dfrac{r}{x}, \\[3mm] Nt = \dfrac{\tau D_T(T_s - T_0)}{\upsilon_f T_\infty},\ Nb = \dfrac{\tau D_B(C_s - C_0)}{\upsilon_f},\ E_c = \dfrac{U^2}{(c_p)_f(T_s - T_0)},\ Br = M\,\mathrm{Pr}, \\[3mm] E = \dfrac{E_a}{k_B T_\infty},\ \lambda = \dfrac{xk_r^2}{U},\ \varepsilon = \dfrac{u_w}{U},\ S_t = \dfrac{c_1}{c},\ S_c = \dfrac{d_1}{d},\ \beta_1 = \dfrac{h_1}{k\left(\dfrac{Ur}{\upsilon x}\right)},\ \beta_2 = \dfrac{h_2}{k\left(\dfrac{Ur}{\upsilon x}\right)} \end{array} \right\} \tag{15}$$
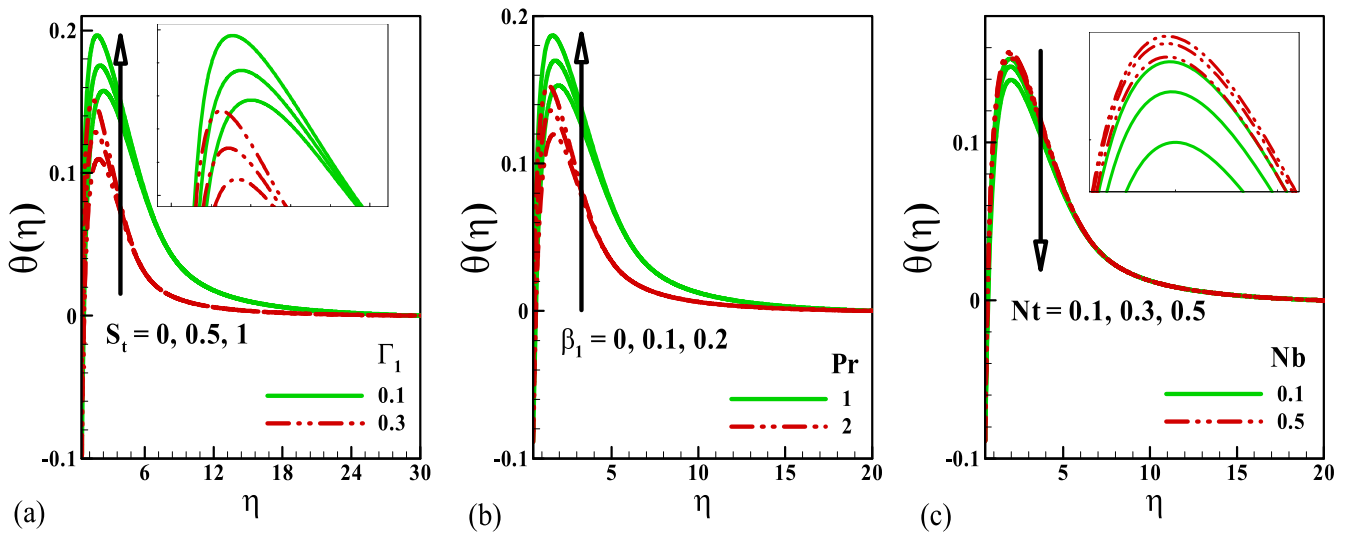
Figure 8. Outcomes of $\theta(\eta)$ versus (a) S_t, Γ_1 (b) β_1, Pr (c) Nt, Nb.
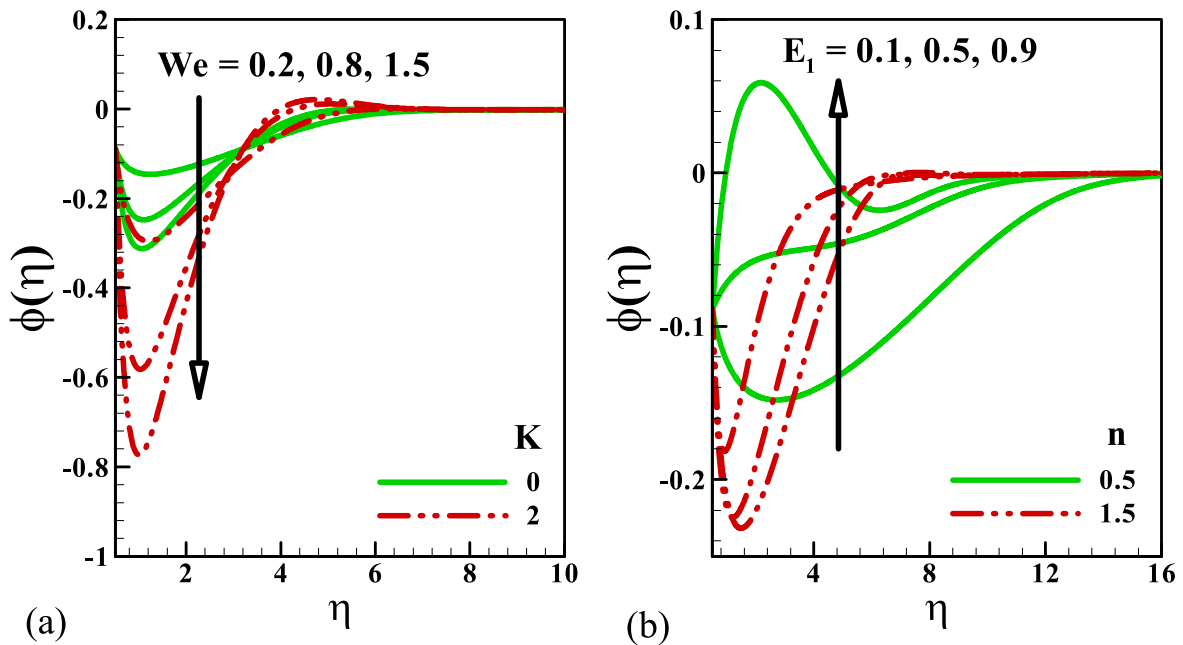

Figure 9. Outcomes of $\phi(\eta)$ versus (a) We, K (b) E_1, n.

In which K stands for material parameter, We for Weissenberg parameter, Gr for thermal Grashof of number, Re_x for Reynolds number, M for Hartman number, E_1 for electric parameter, Pr for Prandtl number, Λ for non-dimensional parameter, Nt for thermophoresis parameter, Nb for Brownian movement parameter, Br for Brinkman number, B for micro-inertia density parameter, Sc for Schmidt number, Γ_1 and Γ_2 for Deborah numbers in terms of relaxation and retardation times respectively, δ for temperature difference parameter, E for dimensionless activation energy, β_1 and β_2 for thermal and solutal Biot numbers correspondingly and S_t and S_c for thermal and solutal stratified parameters correspondingly.

The dimensionless local skin friction and wall couple stresses are defined by

$$Re_x^{\frac{1}{2}} C_{fx} = 4(1 + K)\left(1 + \frac{1}{\beta}\right)A^{\frac{1}{2}}[1 + \{We f''(A)\}^2]^{\frac{n-1}{2}}f''(A) \tag{16}$$

$$Re_x^{\frac{1}{2}} C_{gx} = \left(1 + \frac{K}{2}\right)\left(1 + \frac{1}{\beta}\right)[A^{\frac{1}{2}} g(A) + 2A^{\frac{3}{2}}g_\eta(A)] \tag{17}$$

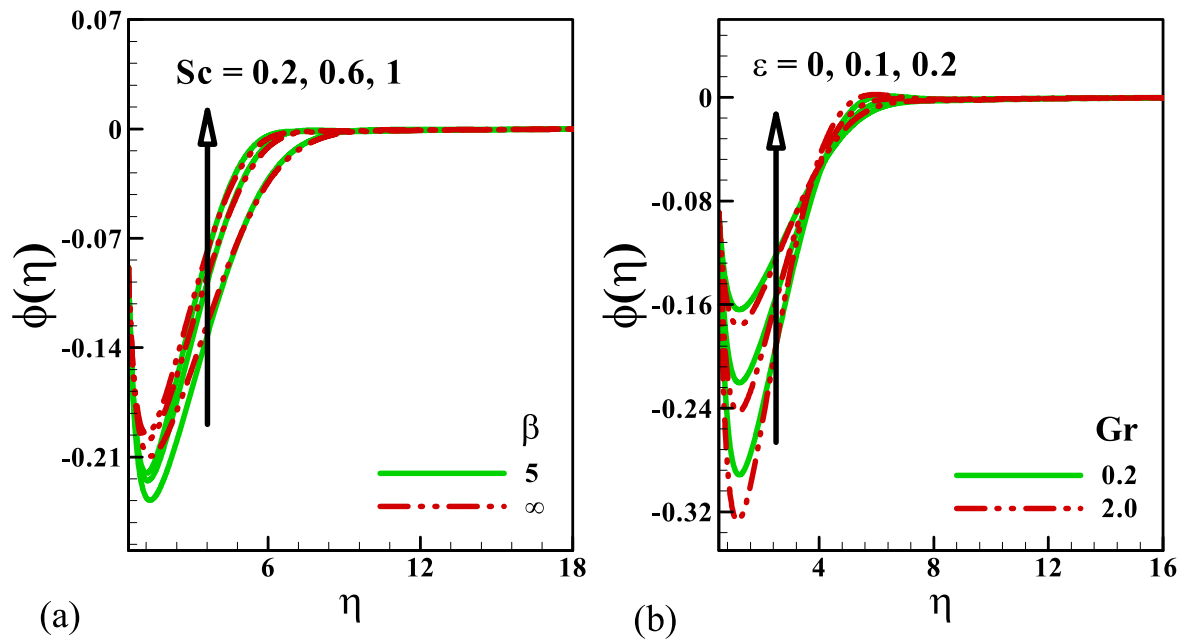in which the local Reynolds number is defined by $Re_x = \frac{Ux}{v}$.

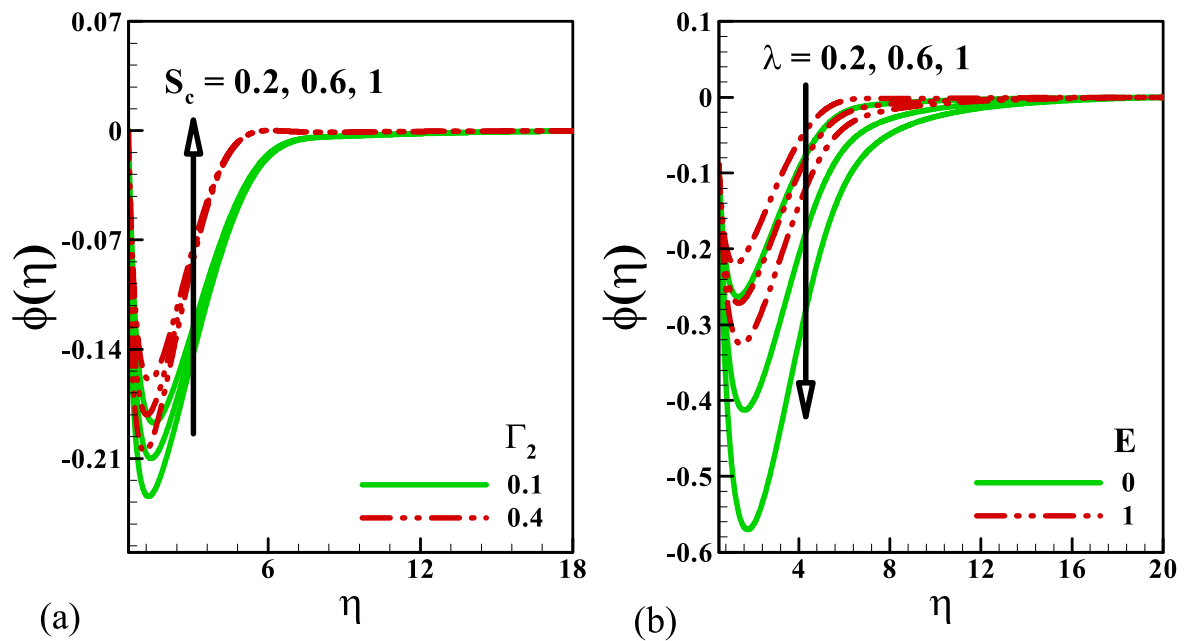**Figure 10.** Outcomes of $\phi(\eta)$ versus (a) *Sc*, β (b) ε, *Gr*.

Figure 11. Outcomes of $\phi(\eta)$ versus (a) S_c, Γ_2 (b) λ, *E*.

3. Numerical outcomes and discussion

Figures 2(a), (b) shows the consequences of Weissenberg number *We*, material parameter *K* and electric parameter E_1 on velocity profile f'. From the figure 2(a), it is seen that velocity profile is diminishing by the variations of Weissenberg number and material parameter. From the figure 2(b), it is also seen that velocity field is decayed for varying electric parameter for both ($n = 0.5$ & 1.5). Figures 3(a), (b) illustrates the behavior of Casson fluid number β, thermal Grashof number *Gr* and Hartman number *M* on velocity profile f'. It is

cleared that the velocity field f' is reduced for growing values of β and *M*. Figures 4(a), (b) designates the influence of Weissenberg number *We*, material parameter *K* and temperature difference parameter δ against velocity profile. It is viewed that velocity is decayed for Weissenberg number *We* while it shows reverse behavior for material parameter *K* and temperature difference parameter δ for both ($n = 0.5$ & 1.5). Figures 5(a), (b) is displayed the characteristics of velocity field for Casson fluid number β, Hartman number *M*, ε and ($m = 0$ & 2). It is noted that velocity field reduces for *M* and ε. The effects of Weissenberg number *We*, material parameter
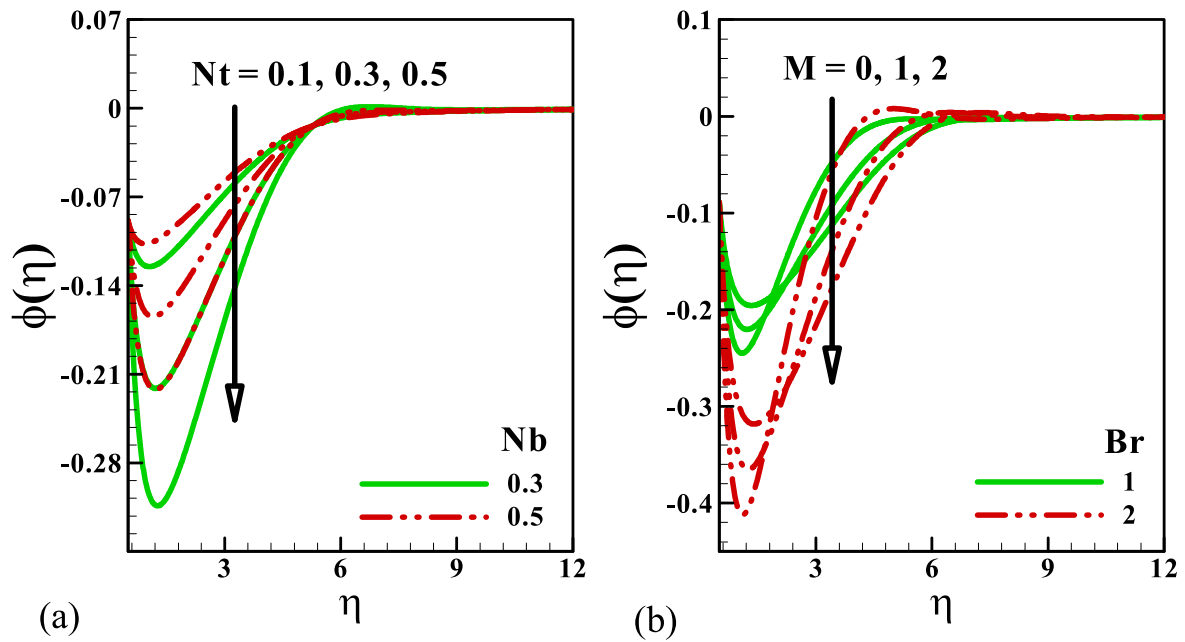
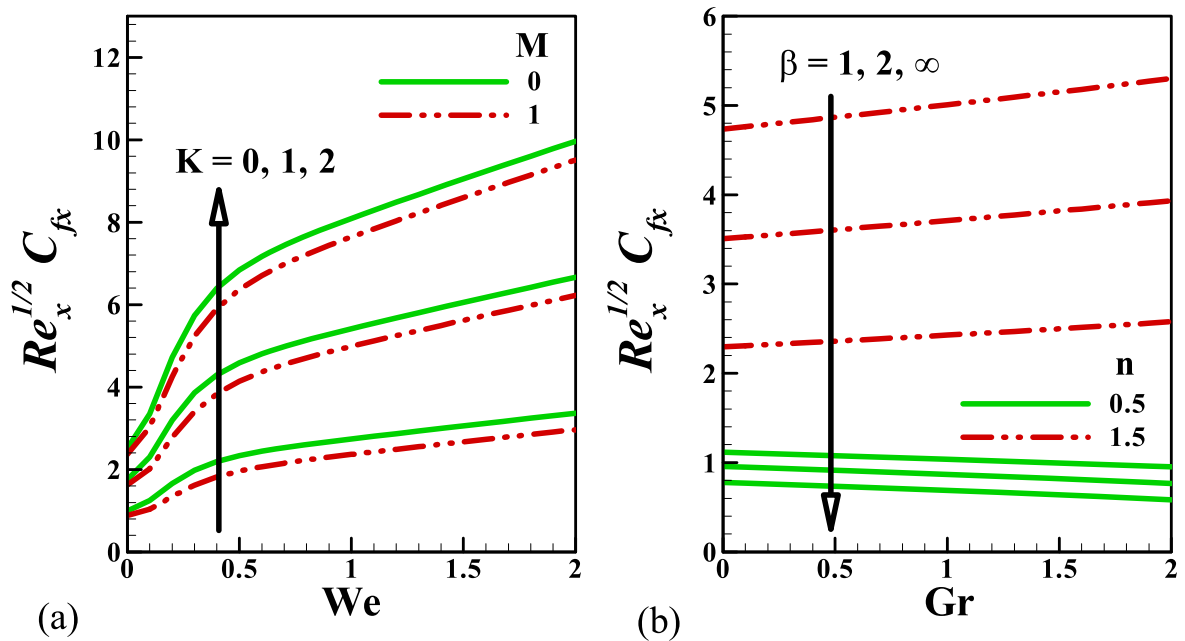**Figure 12.** Outcomes of $\phi(\eta)$ versus (a) *Nt*, *Nb* (b) *M*, *Br*.

Figure 13. Outcomes of skin friction (*x*-direction) (a) *We*, *K*, and *M* (b) *Gr*, *n*, and β.

K and electric parameter E_1 on temperature profile θ are explored in figures 6(a), (b). It is apparent that temperature profile is enlarged for Weissenberg number and material parameter for both ($n = 0.5$ & 1.5). Figures 7(a), (b) signifies the behavior of the thermal Grashof number *Gr*, Hartman number *M*, Casson fluid parameter β and ε on temperature profile θ. It is evaluated that temperature of fluid θ is enhanced for Hartman number and thermal Grashof number. Figures 8(a)–(c) delineates the impacts of Deborah number Γ_1, thermal Biot number β_1, thermal stratification parameter S_t, thermophoresis parameter *Nt*, Prandtl number *Pr* and

Brownian motion parameter *Nb* on temperature profile θ. It is visualized that for the intensifying values of thermal stratification parameter and thermal Biot number β_1, the temperature field enhances. Figures 9(a), (b) discloses the characteristics of Weissenberg number *We*, material parameter *K* and electric parameter E_1 against the concentration of nanoparticles ϕ. It is perceived that concentration of nanoparticles ϕ is augmented with Weissenberg number *We* and material parameter *K* for ($n = 0.5$ & 1.5). The features of the Schmidt number *Sc*, Grashof number *Gr*, Casson fluid parameter β and ε against the concentration of nanoparticles ϕ are
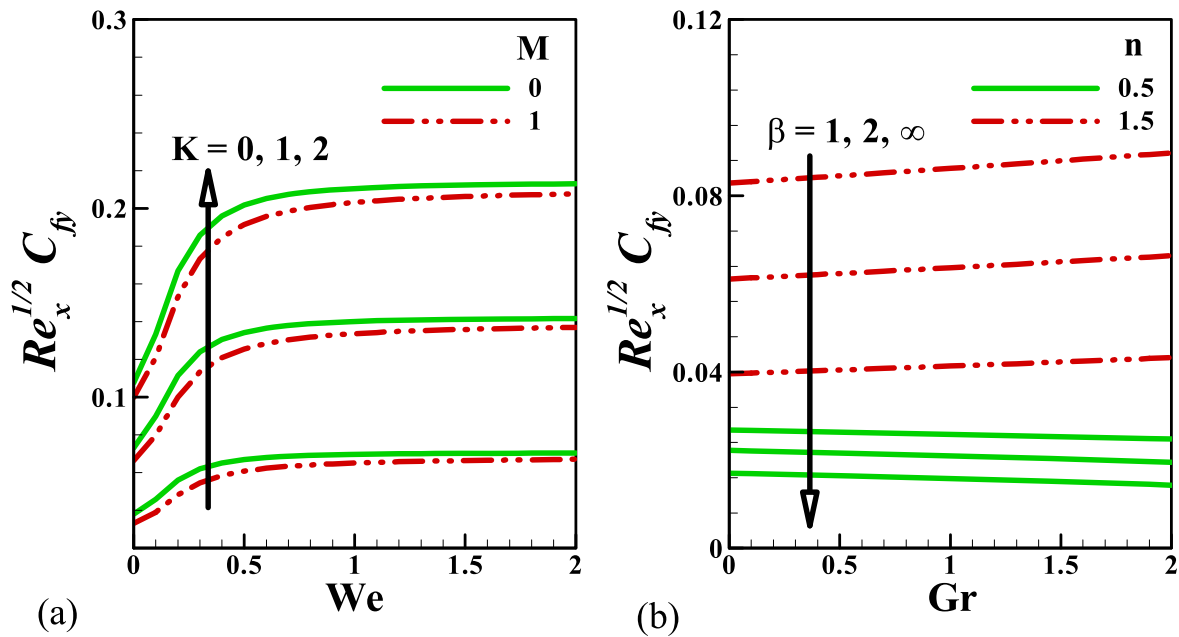
Figure 14. Outcomes of skin friction (*y*-direction) (a) *We*, *K*, and *M* (b) *Gr*, *n*, and β.

Table 1. Numerical values of skin friction for various values of physical parameters.

K	We	β	M	n	$\mathrm{Re}_x^{1/2} C_{fx}$	$\mathrm{Re}_x^{1/2} C_{fy}$
1	0.5	2	1	1.5	4.98998	0.075358
2					7.751786	0.158443
3					10.54131	0.244488
5	0.0				10.55898	0.333666
	0.8				18.32921	0.438883
	1.4				21.32474	0.449830
	0.5	1			21.75952	0.565547
		5			12.79731	0.332377
		10			11.68048	0.303307
		3	0.0		15.12571	0.390802
			0.4		14.77392	0.382630
			0.8		14.44473	0.374891
			1.0	0.5	0.751600	0.033344
				1.0	5.282363	0.188525
				1.5	14.63049	0.360251

explains the outcomes of Hartman number M, Casson fluid parameter β, Weissenberg number We, material parameter K and Grashof number Gr on skin friction $\mathrm{Re}_x^{\frac{1}{2}} C_{fx}$. The skin friction $\mathrm{Re}_x^{\frac{1}{2}} C_{fx}$ increases by expanding values of Weissenberg number and material parameter while reverse situation is watched for Casson fluid parameter for both ($n = 0.5$ & 1.5). Figures 14(a), (b) elucidates the results of Hartman number M, Weissenberg number We, Casson fluid parameter β, material parameter K and Grashof number Gr on skin friction $\mathrm{Re}_x^{\frac{1}{2}} C_{fy}$. The skin friction $\mathrm{Re}_x^{\frac{1}{2}} C_{fy}$ upsurges by escalating values of material parameter. In addition, the skin friction $\mathrm{Re}_x^{\frac{1}{2}} C_{gx}$ is decayed for Casson fluid parameter for both ($n = 0.5$ & 1.5). Numerical outcomes of skin frictions against different values of prominent parameters like K, We, β, M and n are shown in table 1. Here the skin frictions are reduced for various values of M while upsurges for larger estimations of K.

captured in figures 10(a), (b). It has been scrutinized that the concentration profile of nanoparticles is decayed for distinct values of Schmidt number. Figures 11(a), (b) depicts the nature of solutal stratification parameter S_c, Deborah number Γ_2, λ and activation energy E against the concentration of nanoparticles ϕ. It is deliberated from these drawn lines that the concentration of nanoparticles ϕ is upgraded for solutal stratification parameter. The consequences of Hartman number M, thermophoresis parameter Nt, Brownian motion parameter Nb and Brinkman number Br against the concentration profile ϕ are displayed in figures 12(a), (b). It is watched from the curves that the growing values of Hartman number and thermophoresis parameter produces enhancement in concentration profile of nanoparticles. Figures 13(a), (b)

4. Conclusions

Electromagnetohydrodynamic (EMHD) flow of non-Newtonian nanoliquids over thin needle with Robinson's conditions and Arrhenius pre-exponential factor law is studied. The relevant partial differential equations are reformulated into the system of ordinary differential expressions by implementing appropriate transformations. Such obtained equations subject to boundary constraints are computed numerically by considering Runge–Kutta-Fehlberg method. With an enhancement in Hartman number, both velocities decay. The velocity field is upgraded for electric parameter. Temperature field enhances for larger thermal Biot number. The volumetric

concentration of nanoparticles is decayed with Schmidt number. The concentration field upsurges with growing values of thermophoresis parameter while fall down with Brownian movement parameter.

Conflict of interest

The authors declare no conflict of interest.

ORCID iDs

Fazle Mabood https://orcid.org/0000-0003-2698-8427

References

[1] Choi S U S and Eastman J A 1995 Enhancing thermal conductivity of fluids with nanoparticles *ASME International Mechanical Engineering Congress & Exposisition (San Francisco)* (American Society of Mechanical Engineers)

[2] Buongiorno J 2006 Convective transport in nanofluids *Journal of Heat Transfer* **128** 240–50

[3] Ali M, Sultan F, Khan W A, Shahzad M and Arif H 2020 Important features of expanding/contracting cylinder for Cross magneto-nanofluid flow *Chaos, Solitons & Fractals* **133** 109656

[4] Na W, Shah N A, Tlili I and Siddique I 2020 Maxwell fluid flow between vertical plates with damped shear and thermal flux: free convection *Chin. J. Phys.* **65** 367–76

[5] Ahmed A, Khan M and Ahmed J 2020 Mixed convective flow of Maxwell nanofluid induced by vertically rotating cylinder *Applied Nanoscience* **2020**

[6] Khan M I, Nigar M, Hayat T and Alsaedi A 2020 On the numerical simulation of stagnation point flow of non-Newtonian fluid (Carreau fluid) with Cattaneo-Christov heat flux *Comput. Methods Programs Biomed.* **187** 105221

[7] Tlili I, Naseer S, Ramzan M, Kadry S and Nam Y 2020 Effects of chemical species and nonlinear thermal radiation with 3D maxwell nanofluid flow with double stratification—an analytical solution *Entropy* **22** 453

[8] Khan M, Ahmed A and Ahmed J 2020 Boundary layer flow of Maxwell fluid due to torsional motion of cylinder: modeling and simulation *Applied Mathematics and Mechanics* **41** 667–80

[9] Riaz M B and Iftikhar N 2020 A comparative study of heat transfer analysis of MHD Maxwell fluid in view of local and nonlocal differential operators *Chaos, Solitons & Fractals* **132** 109556

[10] Farhangmehr1 V, Moghadasi2 H and Asiaei S 2019 A nanofluid MHD flow with heat and mass transfers over a sheet by nonlinear boundary conditions: heat and mass transfer's enhancement *J. Cent. South Univ.* (2019) **26** 1205–17

[11] Hayat T, Saleem N and Ali N 2010 Effect of induced magnetic field on peristaltic transport of Carreau fluid *Commun. Nonlinear Sci. Numer. Simul.* **15** 2407–23

[12] Ellahi R, Hussain F, Abbas S A, Sarafraz M M, Goodarzi M and Shadloo M S 2020 Study of two-phase newtonian nanofluid flow hybrid with hafnium particles under the effects of slip *Inventions* **5** 6

[13] Shafee A, Arabkoohsar A, Sheikholeslami M, Jafaryar M, Ayani M, Nguyen-Thoi T and Li Z 2020 Numerical simulation for turbulent flow in a tube with combined swirl flow device considering nanofluid exergy loss *Physica.* A **542** 122161

[14] Iftikhar N, Baleanu D, Husnine S M and Shabbir K 2019 Magnetohydrodynamic mixed convection flow of Jeffery fluid with thermophoresis, Soret and Dufour effects and convective condition *AIP Adv.* **9** 035251

[15] Raza J 2019 Thermal radiation and slip effects on magnetohydrodynamic (MHD) stagnation point flow of Casson fluid over a convective stretching sheet *Propulsion and Power Research* **8** 138–46

[16] Sheikholeslami M, Arabkoohsar A and Ismail K A 2020 Entropy analysis for a nanofluid within a porous media with magnetic force impact using non-Darcy model *Int. Commun. Heat Mass Transfer* **112** 104488

[17] Ellahi R, Hussain F, Abbas S A, Sarafraz M M, Goodarzi M and Shadloo M S 2020 Study of two-phase Newtonian nanofluid flow hybrid with Hafnium particles under the effects of slip *Inventions.* **5** 6

[18] Hsiao K L 2016 Stagnation electrical MHD nanofuid mixed convection with slip boundary on a stretching sheet *Appl. Therm. Eng.* **98** 850–61

[19] Nayak M K 2017 MHD 3D flow and heat transfer analysis of nanofluid by shrinking surface inspired by thermal radiation and viscous dissipation *Int. J. Mech. Sci.* **125** 185–93

[20] Nayak M K, Mehmood R, Makinde O D, Mahian O and Chamkha A J 2019 Magnetohydrodynamic flow and heat transfer impact on ZnO-SAE50 nanolubricant flow due to an inclined rotating disk *J. Central South Univ.* **26** 1146–60

[21] Nayak M K, Shaw S and Chamkha A J 2019 MHD free convective stretched flow of a radiative nanofluid inspired by variable magnetic field *Arab. J. Sci. Eng.* **44** 1269–82

[22] Ahmad M, Muhammad T, Ahmad I and Aly S 2020 Time-dependent 3D flow of viscoelastic nanofluid over an unsteady stretching surface *Physica A: Statistical Mechanics and its Applications* **551** 124004

[23] Li F, Sheikholeslami M, Dara R N, Jafaryar M, Shafee A, Nguyen-Thoi T and Li Z 2020 Numerical study for nanofluid behavior inside a storage finned enclosure involving melting process *J. Mol. Liq.* **297** 111939

[24] Nayak M K, Shaw S, Ijaz Khan M, Pandey V S and Nazeer M 2020 Flow and thermal analysis on Darcy-Forchheimer flow of copper-water nanofluid due to a rotating disk: a static and dynamic approach *J Mater Res Technol.* **9** 7387–408

[25] Waqas H, Khan S U, Imran M and Bhatti M M 2019 Thermally developed Falkner–Skanbioconvection flow of a magnetized nanofluid in the presence of a motile gyrotactic microorganism: Buongiorno'snanofluid model *Phys. Scr.* **94** 115304

[26] Muhammad T, Waqas H, Khan S A, Ellahi R and Sait S M 2020 Significance of nonlinear thermal radiation in 3D Eyring–Powell nanofluid flow with Arrhenius activation energy *J. Therm. Anal. Calorim.* **4** 1–6

[27] Li Y, Waqas H, Imran M, Farooq U, Mallawi F and Tlili I 2020 A numerical exploration of modified second-grade nanofluid with motile microorganisms, Thermal Radiation, and Wu's Slip *Symmetry.* **12** 393

[28] Nayak M K, Wakif A, Animasaun I L and Saidi Hassani Alaoui M 2020 Numerical differential quadrature examination of steady mixed convection nanofluid flows over an isothermal thin needle conveying metallic and metallic oxide nanomaterials: a comparative investigation *Arab. J. Sci. Eng.* **45** 5331–46

[29] Dogonchi A S, Nayak M K, Karimi N, Chamkha A J and Ganji D D 2020 Numerical simulation of hydrothermal features of Cu–H_2O nanofluid natural convection within a porous annulus considering diverse configurations of heater *J. Therm. Anal. Cal.* **141** 2109–25

[30] Khan N B, Khan M I, Khan W A and Nayak M K 2020 Physical importance of entropy generation in fluid flow (Williamson) with non linear radiative heat flux *Indian J. Phy.* (https://doi.org/10.1007/s12648-020-01728-0)

[31] Abbasi F M, Shanakhat I and Shehzad S A 2019 Analysis of entropy generation in peristaltic nanofluid flow with Ohmic heating and Hall current *Phys. Scr.* **94** 025001

[32] Gul M, Abbasi F M, Shehzad S A and Shafee A 2020 Entropy generation for peristaltic motion of Carreau's fluid with mixture of ethylene glycol and boron-nitride nanoparticles *Phys. Scr.* **95** 035212

[33] Ramesh G K, Shehzad S A, Rauf A and Chamkha A J 2020 Heat transport analysis of aluminum alloy and magnetite graphene oxide through permeable cylinder with heat source/sink *Phys. Scr.* **95** 095203